Single-frequency optical parametric oscillator intracavity-pumped by a visible VECSEL for low-noise down-conversion to 1.55 μm

STEVEN ANDERSON,[*] ⓘ PAULO HISAO MORIYA, ⓘ LUCIA CASPANI, AND JENNIFER E. HASTIE ⓘ

Institute of Photonics, Department of Physics, SUPA, University of Strathclyde, 99 George Street, Glasgow G1 1RD, United Kingdom
[*]*steven.anderson@strath.ac.uk*

Abstract: We report, to the best of our knowledge, the first optical parametric oscillator (OPO) pumped by a visible AlGaInP-based vertical-external-cavity surface-emitting laser (VECSEL). Tunable emission over 1155–1300 nm in the signal and 1474–1718 nm in the idler are observed by temperature adjustment of a 40 mm-long 5%-MgO:PPLN crystal intracavity-pumped at 690 nm. When optimized for low oscillation threshold, and by implementing resonant idler output-coupling ($T_{OC} = 1.7\%$), extracted output powers of 26.2 mW (signal) and 5.6 mW (idler; one-way) are measured, corresponding to a total down-conversion efficiency and extraction efficiency of 70.2% and 43%, respectively. Further, a total down-conversion efficiency of 72.1% is achieved in the absence of idler output-coupling. Of particular interest for high-precision applications, including quantum optics experiments and squeezed light generation, high stability and single-frequency operation are also demonstrated. We measure RMS stabilities of 0.4%, 1.8% and 2.3% for the VECSEL fundamental, signal and idler, with (resolution-limited) frequency linewidths of 2.5 MHz (VECSEL) and 7.5 MHz (signal and idler).

1. Introduction

Stable, highly correlated, continuous-wave (CW) light beams exhibiting minimal intensity noise and quantum phase noise are of interest for the technological exploitation of quantum correlations and quantum light state applications, in particular for the generation of squeezed states of light [1–4]. Optical parametric oscillators (OPOs), nonlinear devices that have found applications in high-resolution spectroscopy [5,6] and sensitive trace-gas detection [7,8] due to their ability to cover wide spectral regions with narrow linewidths and high output powers, are currently being utilized for targeting squeezed light states [3,9] because of their ability to generate signal and idler photons with non-classical correlations; taking advantage of the $\chi^{(2)}$ nonlinear process of optical parametric down-conversion (PDC). However, although OPOs have become the primary source of generating sub-Poissonian light over the past 30 years [10], targeting intensity-difference squeezing has proven to be extremely difficult when pumping an OPO with a laser exhibiting relaxation oscillations [11]. While solid-state lasers, with their watt-level output power, are generally excellent OPO pump sources for most applications, their quasi-continuous bursts of amplitude fluctuations deem them unsuitable for intracavity generation of intensity-difference squeezed light, particularly at low intensity noise frequencies [12].

In this context, vertical-external-cavity surface-emitting-lasers (VECSELs) [13–15], also known as semiconductor disk lasers (SDLs), are ideal candidates to operate as the pump source for OPOs (see e.g. [12]), especially for the generation of squeezed states of light: their upper-state lifetimes are several orders of magnitude shorter than those of solid-state gain media, typically

between 1-10 ns, and are shorter than the cavity photon lifetime, such that any relaxation oscillations occurring above OPO threshold are critically damped (so-called class A dynamics) [12,16]. Furthermore, their unique amalgamation of high single-mode output power, very low spontaneous emission factor – in comparison to edge-emitting semiconductor lasers, and very high-finesse cavities, permit the VECSEL technology to operate with Schawlow-Townes-Henry (STH) linewidths of the order of mHz [17]. Moreover, due to the vertical geometry of the semiconductor gain structure, where the quantum wells are positioned at the anti-nodes of the optical field standing wave for a process known as resonant periodic gain [18], spatial hole-burning is avoided, thereby enabling stable, low-noise, single-frequency operation in a simple linear cavity arrangement, as opposed to a ring oscillator [19]. VECSELs also provide access to an open, high-finesse, external cavity architecture, with multi-watt-level intracavity powers, even when commercial diode lasers with limited brightness are used as the pump source. This characteristic enables use of the intracavity OPO concept, where the oscillation thresholds can be significantly reduced in comparison to externally-pumped OPO systems, since the OPO crystal can be easily incorporated within the high-finesse cavity of the OPO pump laser. Therefore, the very high mechanical stability requirements inherent in doubly-resonant OPOs (DROs), triply-resonant OPOs (TROs), and pump-enhanced OPOs (PE-OPOs) [20] can be avoided by designing the OPO to operate where only one of the down-converted fields is made resonant (SRO). In this configuration, the higher oscillation threshold can be easily reached and, in addition, the alignment and tunability of the SRO will be far more straightforward in comparison to DRO, TRO, and PE-OPO systems. The first demonstration of a VECSEL-pumped OPO was carried out by Stothard et al. [12], delivering a total down-conversion efficiency (down-converted power) of 83.3% (1.25 W) by pumping the OPO with a 1060 nm InGaAs-based VECSEL system to reach the midinfrared.

In this paper, we report, to the best of our knowledge, the first intracavity OPO pumped by a visible VECSEL, achieving single-frequency operation for all three interacting wavelengths in the intracavity singly resonant OPO (ICSRO). Enabling single-frequency operation enhances the overall performance of the ICSRO beyond that achieved by Stothard and co-workers [12] both in terms of stability and, more importantly, for future implementation of active stabilization techniques; vital for noise reduction for targeting quantum states of light. The SRO system is based upon a 5%-mol magnesium-oxide-doped periodically-poled LiNbO$_3$ (MgO:PPLN) nonlinear crystal positioned at an intracavity focus of the VECSEL fundamental circulating field, oscillating at wavelengths near 690 nm, for signal and idler wavelengths around 1.24 and 1.55 µm. The generation of quantum states of light in the telecom O and C bandwidths (1.3 µm and 1.55 µm, respectively), enabled by the use of a visible VECSEL, is particularly important for applications in quantum communications - to exploit the existing fibre network infrastructure and optoelectronic components - and quantum sensing. Here, a full characterization of the power, efficiency, tuning, and spectral performance of the ICSRO system is demonstrated in the presence and absence of output-coupling (OC) of the resonant idler wave (referred to as OC-idler and HR-idler, respectively). A comparison of the passive stability of the SRO system for two scenarios – when the VECSEL is oscillating with multiple longitudinal modes or on a single mode – is also presented, and clearly demonstrates the advantage of the latter, with an RMS stability of 1.8% and 2.3% measured for the signal and idler, respectively.

2. AlGaInP-based VECSEL-pumped ICSRO configuration

2.1. VECSEL gain structure and external cavity

The configuration of the AlGaInP-based VECSEL-pumped ICSRO system is shown in Fig. 1(a), with the SRO resonant idler cavity internal to the VECSEL cavity. The VECSEL periodic gain structure is similar to those reported previously by our group [17]. It employs pairs of compressively-strained GaInP quantum wells positioned at the field anti-nodes, tensile-strained

compensation layers, and lattice-matched AlGaInP barrier layers grown on top of an AlGaAs/AlAs distributed Bragg reflector (DBR) mirror on a GaAs substrate.
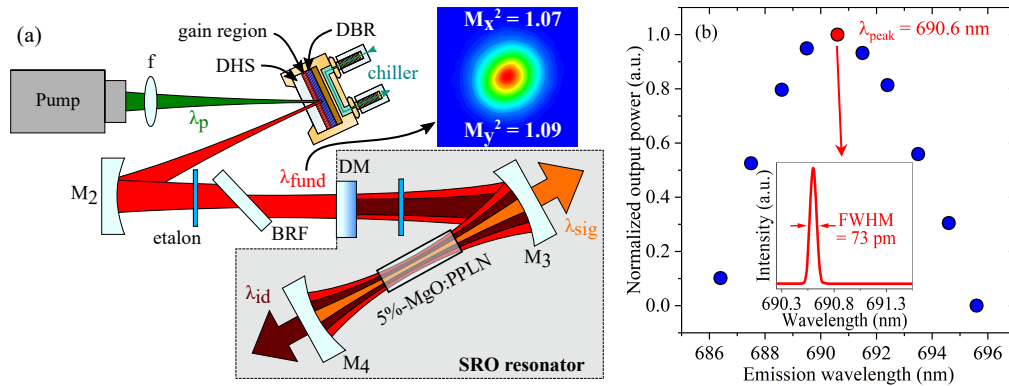

Fig. 1. (a) Schematic (not to scale) of the AlGaInP-based VECSEL-pumped ICSRO experimental set-up, with output-coupling for the resonant idler. The VECSEL (DBR-M2-M3-M4) and the SRO resonant idler (DM-M3-M4) cavities are collinear, with the latter including a 5%-mol magnesium-oxide-doped periodically-poled LiNbO$_3$ (MgO:PPLN) nonlinear crystal. The free-spectral-range (FSR) of the VECSEL and SRO cavities are 365 MHz and 565 MHz, respectively. Inset: VECSEL fundamental beam profile, showing $M^2 = 1.07$ for the x-axis (horizontal) and $M^2 = 1.09$ for the y-axis (vertical), measured using a commercial CMOS camera (Thorlabs DCC1545 M). (b) Tunability of the AlGaInP-based VECSEL output spectrum via rotation of a quartz birefringent filter (BRF). Inset: Full-width at half-maximum (FWHM) linewidth measurement of the AlGaInP-based VECSEL spectrum at $\lambda_{fund} = 690.6$ nm. f: lens; DBR: distributed Bragg reflector; DHS: diamond heatspreader; DM: dichroic mirror; λ_p, λ_{sig}, λ_{id}: VECSEL pump (diode-pumped solid-state laser; DPSSL), signal and idler wavelengths at 532, 1245.2 and 1550.8 nm, respectively.

A 4×4 mm^2 gain structure sample is capillary-bonded to a single crystal diamond heatspreader for thermal management and mounted on a temperature-stabilized brass mount. The VECSEL sample is then positioned at one end of a 4-mirror standing-wave Z-cavity formed by the DBR and cavity mirrors M$_2$, M$_3$ and M$_4$ (see Fig. 1(a)), with radii of curvature of 75, 75 and 50 mm, respectively. All VECSEL cavity mirrors are chosen to be highly reflective (HR, R > 99.995%) at 670-710 nm to ensure maximum intracavity circulating power. Laser oscillation at 690.6 nm is achieved in a single transverse mode when the gain structure is optically-pumped by a commercial 532 nm diode-pumped solid-state laser (DPSSL, Coherent Verdi V5). Wavelength tunability of 10 nm is obtained by inserting a 4 mm-thick quartz plate oriented at Brewster's angle (see Fig. 1(b)) as a birefringent filter (BRF).

2.2. SRO crystal and ICSRO resonator

A MgO:PPLN SRO crystal, with dimensions of $40 \times 10 \times 0.5$ mm^3 and a MgO doping concentration of 5%-mol (fabricated by Covesion Ltd), is electric-field-poled using nine different grating periods ranging from 13.83-17.10 μm along the crystal's y-axis. The crystal end facets are anti-reflection (AR) coated for the VECSEL fundamental (R$_{fund}$ < 0.2%), signal (R$_{sig}$ < 2%) and idler wavelengths (R$_{id}$ < 2%). The SRO crystal is mounted at a 90° angle to the resonator plane, enabling type-0 quasi-phase-matching (QPM) [21,22], and is housed within a temperature-stabilized oven, which enables tuning of the crystal temperature over the range of 30-200 °C.

The SRO resonant idler cavity is formed within that of the VECSEL by the insertion of a dichroic beamsplitter mirror (DM) that is highly transmissive (HT, R$_{fund}$ < 0.5%) at the VECSEL

fundamental wavelength but HR ($R_{id} > 99.99\%$ for 0° incidence) around the idler wavelengths (1500-1600 nm). Two different regimes were used to characterize the VECSEL-pumped ICSRO performance: OC-idler and HR-idler. In the former, the resonant idler wavelength is partially coupled out of the SRO cavity via mirror M_4 ($T_{OC} = 1.7\%$), while the non-resonant signal is highly-reflected at mirror M_4 ($R_{sig} > 99\%$) and exits the cavity via mirror M_3 ($R_{sig} < 2\%$) after a double-pass of the MgO:PPLN crystal. For the latter, the signal exits the cavity via M_4 ($R_{sig} < 2\%$) after a single-pass through the MgO:PPLN crystal, while the idler is highly-reflected at all SRO cavity mirrors DM, M_3 and M_4 ($R_{id} > 99.9\%$). The confocally-focused VECSEL fundamental and resonant idler beam waists at the center of the MgO:PPLN crystal are weakly astigmatic, measuring 48.7 μm and 67.0 μm, respectively, for the 40 mm-long crystal length, corresponding to focusing parameters of $\xi_p = 1.09$ and $\xi_i = 0.99$ which, according to Guha et al. [23,24], are close to the minimum oscillation threshold condition.

The insertion of two fused-silica etalon filters, one 300 μm-thick within the VECSEL branch and one 200 μm-thick within the SRO branch of the ICSRO resonator (see Fig. 1(a)), forces the SRO pump laser to operate with a (resolution-limited) spectral width of 73 pm (see Fig. 1(b), inset); measured with an Optical Spectrum Analyser (Anritsu MS9710C) to be well within the pump acceptance bandwidth [25] of the ICSRO system of 126 pm.

3. Experimental results and analysis

3.1. ICSRO spectra and tuning characteristics of the SRO

The VECSEL fundamental, signal and idler wavelength emission peaks are measured to be 690.6, 1245.2 and 1550.8 nm (see Fig. 2(a)), respectively, corresponding to a MgO:PPLN grating period of $\Lambda = 14.55$ μm and a MgO:PPLN crystal temperature of 114 °C. Tuning of the SRO is performed by varying the MgO:PPLN crystal temperature over the range of 90-180 °C (see Fig. 2(b)), resulting in signal and idler tuning ranges of 145 nm (1300-1155 nm) and 244 nm (1474-1718nm), respectively, corresponding to a signal (idler) tuning rate of 1.6 nm/°C (2.7 nm/°C). A theoretical curve, based on the temperature-dependent Sellmeier equation proposed by Gayer et al. [26], also shown in Fig. 2(b), is in excellent agreement with the experimentally observed results.
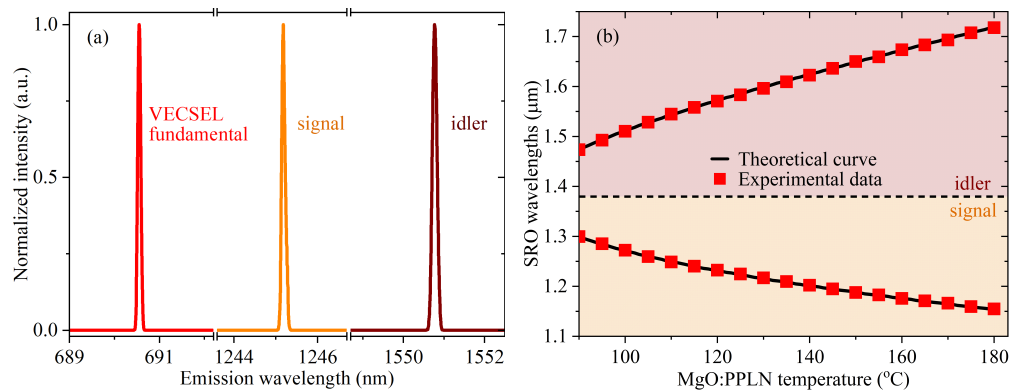

Fig. 2. (a) Normalized intensity spectra of the VECSEL fundamental, signal and idler centered at 690.6, 1245.2 and 1550.8 nm, measured using an Optical Spectrum Analyzer (OSA; Anritsu MS9710C; resolution - 0.05 nm). (b) Temperature tuning curve of the SRO, measured using the 14.55 μm poling period of the MgO:PPLN crystal and pumped at $\lambda_{fund} = 690.6$ nm. Solid curve: theoretical tuning curve calculated via [26].

3.2. HR-idler ICSRO power and efficiency performance

Figure 3(a) demonstrates the power and efficiency performance of the HR-idler ICSRO system as a function of DPSSL power absorbed by the VECSEL gain structure. At the maximum absorbed DPSSL power, before the onset of thermal rollover, at around 2.96 W, the (one-way) extracted signal power is 14.2 mW. Figure 3(a) also shows the total down-converted power, defined as $P_{DC} = 2\frac{P_{sig}}{\eta_{sig}}\left(1 + \frac{\lambda_{sig}}{\lambda_{id}}\right)$, where P_{sig} is the (one-way) extracted signal output power and η_{sig} is the signal field coupling efficiency within the SRO cavity, taking into account the transmission loss experienced by the signal field at mirror M_4 and the reflection loss of the signal field at the end facets of the MgO:PPLN crystal. After accounting for the dual-direction signal generation, the quantum defect between the signal (λ_{sig}) and idler (λ_{id}) wavelengths, and the signal field coupling efficiency ($\eta_{sig} \sim 96\%$), the total down-converted power is 53.3 mW.
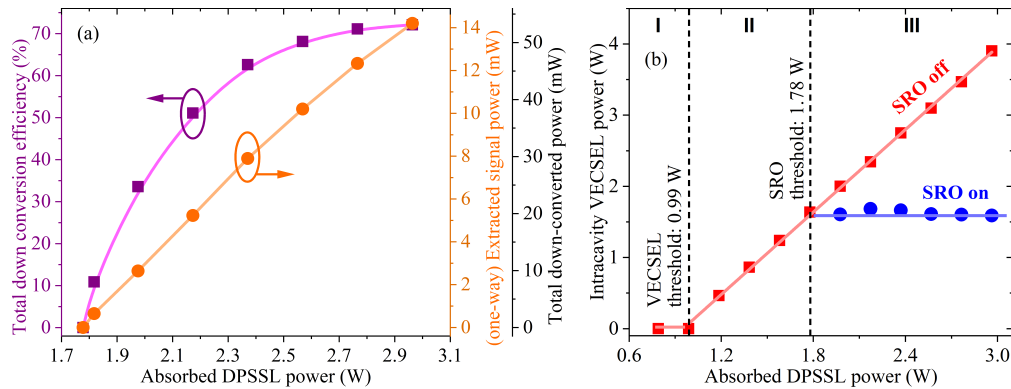

Fig. 3. (a) Extracted (one-way) signal power (orange circles) and estimated ICSRO down-converted efficiency (purple squares) for increasing increments of absorbed DPSSL power. (b) Measured VECSEL intracavity (circulating) power as a function of absorbed DPSSL power in the presence (blue circles) and absence (red squares) of PDC. Regions I, II, and III correspond to "below VECSEL threshold", "between VECSEL and SRO threshold", and "above SRO threshold", respectively.

The intracavity VECSEL power, i.e., the VECSEL power circulating within the ICSRO resonator, is plotted as a function of absorbed DPSSL power (see Fig. 3(b)). Upon examination of this figure, the VECSEL and SRO thresholds occur at an absorbed DPSSL power of 0.99 W and 1.78 W, respectively. At SRO threshold, the VECSEL intracavity power is estimated to be 1.59 W, in very good agreement with the ICSRO threshold condition, outlined in [27], and calculated to be 1.54 W. This implies that the ICSRO resonator is well-aligned and optimized in comparison to the designed configuration and that the laser cavity optics' coatings specifications are accurate. Furthermore, Fig. 3(b) also demonstrates the three well-defined regions of ICSRO operation, with distinct evidence of the "pump-clamping" effect [27,28]: below VECSEL threshold (I), between VECSEL and SRO thresholds (II), and above SRO threshold (III). The linear relationship observed between the VECSEL intracavity field and the absorbed DPSSL power in the absence of PDC, as well as the expected "clamping" behavior of the VECSEL intracavity field above SRO threshold, serve to emphasize efficient mode-matching and strong optimized alignment concurrent within the ICSRO system.

It is worth noting that the ICSRO is operating at 1.7 times threshold and at 92.5% of the optimum pumping level of 3.2 W, estimated using $P_{th}^{SRO} = (P_{th}^{fund} \cdot P_p)^{1/2}$ [28], as set by the thresholds of the VECSEL (P_{th}^{fund}) and SRO (P_{th}^{SRO}), and the absorbed DPSSL power P_p. Therefore, the ICSRO system is only required to be operated at 1.8 times threshold to reach an optimal down-conversion

efficiency, while all external-cavity OPOs require being pumped at 2.47 times threshold to reach an optimal down-conversion efficiency [29]. Estimating the ICSRO down-conversion efficiency is achieved by comparing the total down-converted power to the output power that could be usefully coupled out of the VECSEL when PDC is suppressed. This is accomplished by introducing optimum output-coupling at the VECSEL fundamental wavelength while maintaining all intracavity components in place within the ICSRO resonator. For this configuration, the optimum OC for the VECSEL fundamental wavelength is $\sim 3\%$, and with the down-conversion process ceased, the VECSEL output power is 74 mW at the maximum absorbed DPSSL power (2.96 W). The estimated total down-conversion efficiency of the ICSRO system is thus calculated to be 72.1% (see Fig. 3(a)).

3.3. OC-idler ICSRO power and efficiency performance

The OC-idler ICSRO power and efficiency performance is characterized by introducing partial output-coupling ($T_{OC} = 1.7\%$) around the idler wavelengths (1500-1600 nm) via mirror M_4. As illustrated in Fig. 4(a), the ICSRO now begins to oscillate at a higher absorbed DPSSL power (and corresponding VECSEL intracavity power) of 2.41 W (1.95 W), 0.63 W higher than the 1.78 W threshold observed in the HR-idler regime (see Fig. 3(b)). We note that, as well as the insertion of the OC-idler mirror, the SRO threshold is increased further by pumping the VECSEL at a different spot on the gain chip. At the maximum absorbed DPSSL power, before the onset of thermal rollover (2.96 W), a (one-way) extracted idler power of 5.6 mW is measured, yielding a useful extraction efficiency of 7.6%. Since the non-resonant signal is now double-passing the MgO:PPLN crystal, a total signal power of 26.2 mW is measured via mirror M_3, delivering a useful extraction efficiency of 35.4%, resulting in a total extraction efficiency of 43% (see Fig. 4(b)). Further improvement of the extraction efficiency of the ICSRO system can be achieved through optimization of the resonant idler output-coupling. Using the new signal field coupling efficiency of $\eta_{sig} \sim 91\%$, achieved by taking into account the transmission loss of the signal field at mirrors M_3 and M_4, as well as the reflection loss of the signal field at both the front and end facet of the MgO:PPLN crystal, a total down-conversion efficiency of 70.2% is estimated based on a calculated total down-converted ICSRO power of 51.9 mW (see Figs. 4(a) and (b)). It is worth noting the total down-converted power is calculated with a factor of 2 reduction, in comparison to the HR-idler regime, due to the non-resonant signal now double-passing the MgO:PPLN crystal.
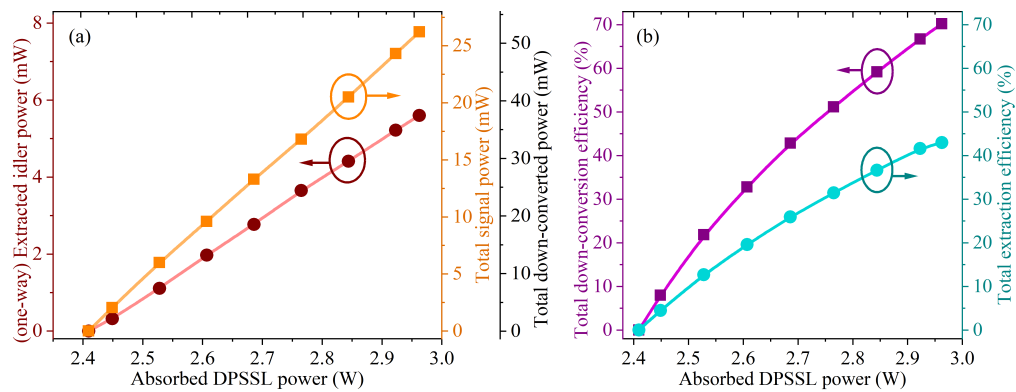

Fig. 4. (a) Extracted (one-way) idler power (brown circles) and measured total signal power (orange squares) for increasing increments of absorbed DPSSL power. (b) Estimated down-converted efficiency (purple squares) and total extraction efficiency (cyan circles) of the ICSRO as a function of absorbed DPSSL power.

3.4. Passive stability characteristics of the SRO pumped in a multi-longitudinal-mode VECSEL

Figure 5(a) shows the short-term passive stability of the VECSEL fundamental power, via the leakage through HR mirror M_3, when the SRO is "switched on" (blue data points) and when the SRO is "switched off" (red data points). The SRO is "switched off" by mis-aligning the SRO cavity via a small tilt of the DM and, subsequently, "switched back on" by reversing the mis-alignment, all without adjusting any other elements within the SRO resonator. For the maximum absorbed DPSSL power, before the onset of thermal rollover, of 2.96 W, and when the VECSEL is operating on multiple longitudinal modes, the passive power stability of the VECSEL is measured over a timescale of 5 ms, using the leakage from mirror M_3. Excellent stability is observed in both regimes; the RMS stability is measured to be 0.86% and 0.96% in the absence and presence of PDC, respectively. The reduction in VECSEL fundamental power above SRO threshold is due to the pump "clamping" effect, mimicking the VECSEL intracavity power behavior outlined in Fig. 3(b). The long-term signal output power is also measured, this time over a timescale of 4000 s, and at an absorbed DPSSL power of 2.69 W, and via OC-mirror M_3 (see Fig. 5(b)). The peak-to-peak and RMS amplitude fluctuations are measured to be no more than 19.8% and 7.0%, respectively. One method to improve the overall passive stability of the ICSRO system is to force the VECSEL to operate on a single-longitudinal-mode, and this is detailed within the next section.
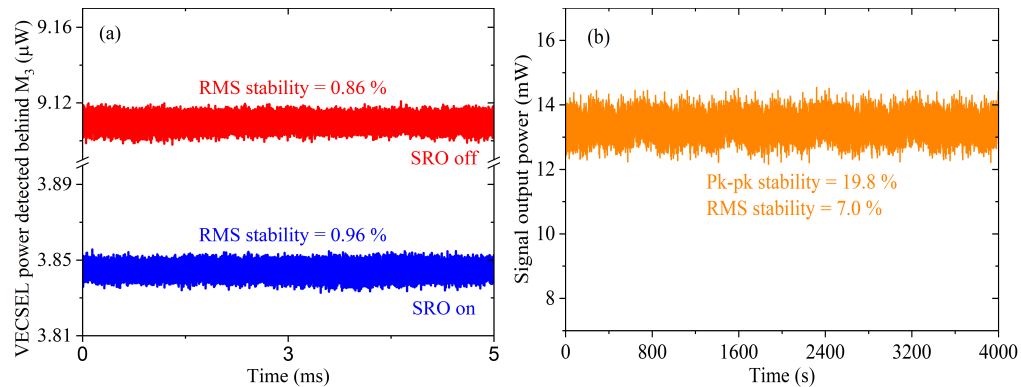

Fig. 5. OC-idler ICSRO passive power stability analysis when the VECSEL is operating on multiple longitudinal modes. (a) Short-term (5 ms) VECSEL power stability, measured via leakage through HR mirror M_3, in the presence (blue data points) and absence (red data points) of PDC, at an absorbed DPSSL power of 2.96 W. (b) Long-term SRO signal power stability, measured over 4000 s via OC-mirror M_3, at an absorbed DPSSL power of 2.69 W. Pk-pk: peak-to-peak, RMS: root-mean-square.

3.5. Spectral and passive stability characteristics of the SRO pumped in a single-frequency VECSEL

Single-frequency operation of the VECSEL fundamental and, consequently, the SRO is achieved by replacing the 200 μm-thick fused silica etalon, incorporated within the SRO branch of the ICSRO resonator, with a 1 mm-thick yttrium aluminuim garnet (YAG) filter. Here, the absorbed DPSSL power is 2.69 W. The VECSEL fundamental, signal and idler transmission spectra, when coupled to their respective scanning Fabry-Perot interferometers (FPIs), are presented in Fig. 6. The visible (and infrared) FPI has a free spectral range (FSR) and finesse of 1 (1.5) GHz and 400 (200), respectively. Narrow, free-running MHz linewidths of each transmission peak are measured, all of which are close to the visible (infrared) FPI resolution limit of 2.5 MHz

(7.5 MHz). Within the range of their respective FPIs, which exceed the FSRs of their respective VECSEL (SRO) cavities of 365 MHz (565 MHz), each interacting field is oscillating on a single frequency peak, thereby indicating that each of the interacting wavelengths of the ICSRO system is operating on a single-longitudinal-mode (see Fig. 6).
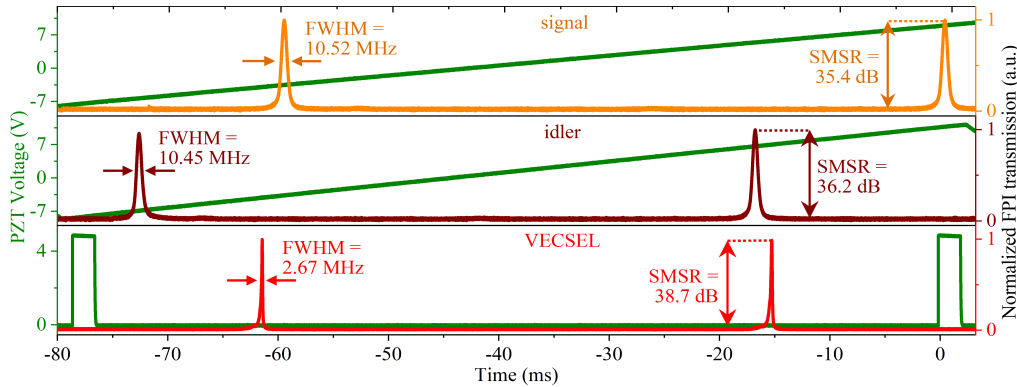

Fig. 6. Normalized Fabry-Perot interferometer (FPI) transmission and reference cavity PZT voltage as a function of time for the VECSEL fundamental, signal and idler wavelengths outlined in Fig. 2(a). The FSR (finesse) of the visible and infrared FPI's were 1 GHz (400) and 1.5 GHz (200), respectively. A sawtooth function is sent to the infrared reference cavity PZT (for signal and idler) and a digital trigger is created by the reference controller for the visible cavity (for the VECSEL). SMSR: side mode suppression ratio, FWHM: full-width at half-maximum.

Finally, at an absorbed DPSSL power of 2.69 W, the long-term passive power stability of the ICSRO system is measured for the VECSEL operating on a single-longitudinal-mode (see Fig. 7). The measurement is recorded over a timescale of 500 s since, as a result of cavity length fluctuations arising from various excess noise components incident on the open cavity (i.e., environmental noise, mechanical noise from optical mounts, and thermal drift), mode-hopping and multi-longitudinal-mode operation is observed over longer time periods. For recording the measurements, the VECSEL output power is recorded from one of the two reflections from the quartz BRF, resulting in a higher output power compared with the short-term VECSEL power stability measured via leakage through HR mirror M_3 (see Fig. 5(a)), while the signal and idler output powers are recorded via mirrors M_3 and M_4, respectively. Excellent passive stability is observed for all three ICSRO interacting wavelengths; RMS stabilities of 0.4%, 1.8% and 2.3% are measured for the VECSEL fundamental, signal and idler, respectively, resulting in a near 4-fold enhancement in the power stability of the ICSRO system in comparison to the multi-longitudinal-mode case (see Fig. 5(b)). The passive power stabilities recorded within the ICSRO system are similar to previously reported single-frequency 1064 nm Yb-fiber pumped CW-SRO systems, and are more than twice as stable as previously reported solid-state-pumped CW-SRO systems that are pumped (single-frequency) in both the infrared, and visible, spectral regions. This is discussed, in detail, in the following section.
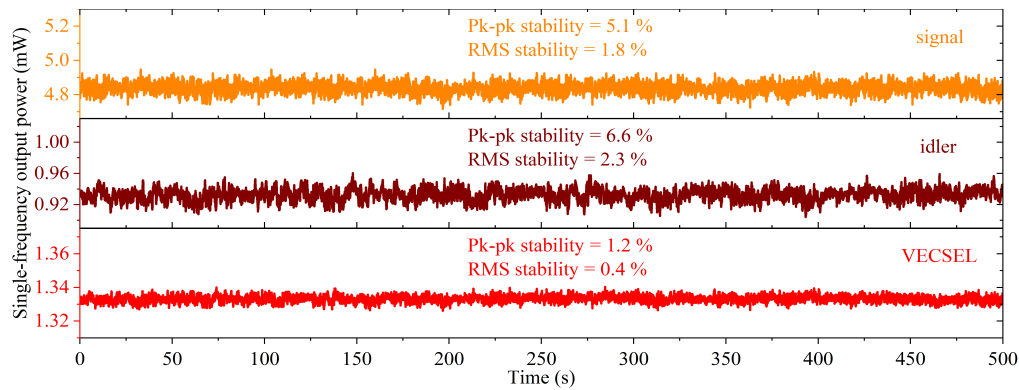
Fig. 7. Single-frequency ICSRO passive power stability, measured over 500 s, at an absorbed DPSSL power of 2.69 W. The single-frequency output powers for the VECSEL fundamental, signal and idler are measured via one of the quartz BRF reflections, and via leakage through mirrors M_3 and M_4, respectively. Pk-pk: peak-to-peak, RMS: root-mean-square.

4. Discussion

To the best of our knowledge, these are the first results to provide direct evidence of single-frequency OPO operation intracavity-pumped by a VECSEL, as the previous results [12,16,30], in particular the work of Hempler et al. [16], present (resolution-limited) FWHM linewidths exceeding the ICSRO resonator FSR. It is important to highlight that the ICSRO results presented are obtained using an open breadboard system and therefore further improvements to the laser operation, in terms of stability and efficiency, are expected to be achieved by, for example, passive stabilization techniques, such as improved laser cavity engineering and packaging. In addition, with improved thermal management of the VECSEL by, for example, pumping the gain medium with a larger spot size to distribute heat more evenly and reduce the power density, further power scaling of the VECSEL can be implemented to extend the point of thermal rollover. This, in turn, would allow the VECSEL-pumped ICSRO system to reach total down-conversion efficiencies exceeding 80%, as achieved by Stothard and colleagues [12], at the expense of a higher VECSEL threshold.

  Despite our ICSRO system being a proof-of-principle breadboard system, the results obtained in comparison to previously reported CW-ICSRO and CW-SRO systems, especially in terms of the total down-conversion efficiency and power stability, highlight the fact that our ICSRO system is well-aligned and operating with near-optimum mode-matching. From an efficiency point of view (see Table 1), efficiencies between 66% and 93% have been achieved using different pump lasers with nonlinear crystals placed in external ring resonators. The 72.1% down-conversion efficiency achieved here is thus competitive, with the added significant advantages of the low noise of the VECSEL. There are two direct methods that we can implement to further enhance the down-conversion efficiency of our ICSRO system towards those mentioned above. The first involves operating the SRO at the theoretically optimal pumping point which, for the HR-idler regime, is at an absorbed DPSSL power of 3.2 W. This can be achieved by increasing the thermal rollover point either by reducing the on-chip chiller temperature or by increasing the DPSSL spot size incident on the VECSEL chip (with a commensurate increase of the intracavity mode size). The alternative method involves optimizing our ICSRO system for high down-conversion efficiency instead of for low oscillation threshold. According to Guha et al. [23,24], this can be achieved by re-designing our ICSRO resonator to reach confocal parameters of $\xi_p = 1.0$ and $\xi_i = 0.9$ at the center of the MgO:PPLN crystal for the VECSEL fundamental and resonant idler, respectively. However, the increase in ICSRO threshold, attributed to this optimization scheme,

requires a DPSSL with higher output powers to reach, or operate close to, the optimal pumping point.

Table 1. CW ICSRO down conversion efficiency comparison. L: length

Pump laser		Crystal		Down conversion efficiency (%)	Ref.
Type	λ (nm)	L (mm)	material		
Fiber-coupled laser diode array	808	30	MgO:aPPLN	93	[31]
Ti:Sapphire	~800	20	KTiOPO$_4$	87	[32]
InGaAs VECSEL	1060	30	MgO:PPLN	83.3	[12]
Fiber laser	976	40	MgO:PPLN	66	[33]
AlGaInP VECSEL	690	40	MgO:PPLN	72.1	This work

In terms of the passive power stability of our ICSRO system, a detailed comparison with previously reported work on CW-SROs is presented in Table 2. Passive RMS stabilities <2% have been reported [34,35] for nonlinear crystals being pumped in external ring cavity geometries. With the exception of the VECSEL, all of the other passive power stabilities reported in the table are also characterized with the SRO embedded within a ring cavity. Comparing to the passive stability performance of our single-frequency ICSRO system, which demonstrated peak-to-peak (RMS) stabilities of better than 6.6% (2.3%) over a sampling time of 500 s for each interacting field, it demonstrates that it is possible to achieve passive stabilities close to single-frequency (infrared) Yb-fiber pumped external CW-SROs despite our SRO system being intracavity-pumped at visible red wavelengths in a standing wave cavity. A key reason for this is due to the resonant periodic gain arrangement of the quantum wells embedded within the VECSEL active gain region, which allows the external cavity to be designed linearly, and hence, more straightforwardly, while maintaining the same stability characteristics of ring resonators. A reason for the increased stability performance compared to both the 532 nm solid-state-pumped CW-SRO system, and the (infrared) all-solid-state-pumped CW-ICSRO system, is due to the minimal thermal lensing effect inherent within VECSEL systems in comparison to solid-state lasers, obtained due to the semiconductor disk nature of the VECSEL active gain medium [37]. Despite the high passive stability performance achieved within our CW-ICSRO system, we note that Zheng et al. [38] demonstrated an RMS stability of 0.19% for over 30 mins without implementing active stabilization techniques. The high stability was achieved by utilizing an angle-polished MgO:PPLN crystal within a ring resonator, along with implementing a Teflon cover for thermal isolation and to protect against air currents. However, with efficient implementation of further passive and active stabilization schemes, we can target passive power stabilities closer to those reported by Zheng et al. [38].

Table 2. CW ICSRO/SRO passive stability comparison. L: length; SF: single-frequency.

Pump laser		Crystal		Passive stability (%)	Time	Ref.
Type	λ (nm)	L (mm)	material			
SF Yb fiber laser	1064	48	MgO:PPLN	1.3 (RMS)	60 s	[34]
SF Yb fiber laser	1064	80	KTiOPO$_4$	1.9 (RMS)	1 h	[35]
Solid state laser	1064	50	Undoped PPLN	5.6 (RMS)	3 h	[30]
Solid state laser	532	30.14	MgO:sPPLT	16 (pk-to-pk)	5 h	[36]
SF AlGaInP VECSEL	690	40	MgO:PPLN	6.6 (pk-to-pk) 2.3 (RMS)	500 s	This work

To fully realize the potential of the VECSEL as an OPO pump source for generating squeezed states of light, active-frequency stabilization of the VECSEL is required to further reduce

the frequency and intensity noise, as well as enhancing the overall efficiency of our ICSRO performance. Most importantly, by reducing the intensity noise of the OPO pump laser, lower amounts of intensity noise will be transmitted into the signal and idler modes, resulting in reduced excess noise within the intensity difference correlations above OPO threshold [39]. Therefore, the superior low intensity noise of the VECSEL, via combination of actively stabilizing the VECSEL fundamental frequency, as well as their ability to operate free of relaxation oscillations (class A dynamics), enables them to be highly promising pump sources for OPOs for targeting intensity-difference squeezed light. It is also important to note that the sub-shot-noise intensity correlations and squeezing levels of below-threshold SROs match those of DROs, yet with the advantage of a simpler experimental realization [40]. Further to the reduction in intensity noise, a significant reduction in quantum phase noise can be achieved by actively stabilizing the VECSEL fundamental frequency. This is relevant since the excess noise in the phase of the OPO pump source is detrimental to the continuous-variable entanglement that can be generated in above threshold OPOs [41]. As well as a reduction in quantum phase noise, ultra-narrow fundamental linewidths can also be reached, with sub-kHz linewidths having already been recently demonstrated within our research group [17,42,43], where identical AlGaInP-based VECSEL samples were utilized. While the degree of intensity-difference squeezing that can be achieved should be irrespective of the quantum phase noise and narrow linewidth operation of the OPO pump source, for a given low intensity noise, reducing these characteristics can still open up new possibilities and applications in e.g., atomic clocks [44], and quantum communication [45], cryptography [46], spectroscopy [47,48] and computing [49].

5. Conclusion

In conclusion, we have demonstrated, for the first time, an intracavity OPO pumped by a visible AlGaInP-based VECSEL, achieving high down-conversion efficiencies of 72.1% and 70.2% in the HR-idler and OC-idler regimes, respectively. The insertion of a 1 mm-thick YAG etalon, along with extensive cavity optimization, permits ICSRO oscillation on a single-longitudinal-mode, demonstrating, to the best of our knowledge, the first direct evidence of a single-frequency OPO pumped by a VECSEL system. Of particular importance for the applications of interest, RMS stabilities of 0.4%, 1.8% and 2.3% were measured for the VECSEL fundamental, signal and idler under single-frequency ICSRO oscillation, demonstrating similar stability performance to that which must typically be achieved using ring resonators for other gain media. Further optimization of the single-frequency ICSRO system is required, via passive stabilization and active-frequency-locking of the VECSEL, to further reduce the intensity and quantum phase noise transmitted into the signal and idler modes, as well as increasing the efficiency of the overall ICSRO performance; vital for high precision applications, and for the generation of quantum squeezed states of light, particularly above OPO threshold.

Disclosures. The authors declare no conflicts of interest.

Data availability. Data related to this publication has been made available at the University of Strathclyde data repository [50].

References

1. C. M. Caves, "Quantum-mechanical noise in an interferometer," Phys. Rev. D **23**(8), 1693–1708 (1981).
2. R. E. Slusher, L. W. Hollberg, B. Yurke, *et al.*, "Observation of squeezed states generated by four-wave mixing in an optical cavity," Phys. Rev. Lett. **55**(22), 2409–2412 (1985).
3. L.-A. Wu, M. Xiao, and H. J. Kimble, "Squeezed states of light from an optical parametric oscillator," J. Opt. Soc. Am. B **4**(10), 1465–1475 (1987).

4. U. L. Andersen, T. Gehring, C. Marquardt, *et al.*, "30 years of squeezed light generation," Phys. Scr. **91**(5), 053001 (2016).

5. J. Krieg, A. Klemann, I. Gottbehüt, *et al.*, "A continuous-wave optical parametric oscillator around 5-μm wavelength for high-resolution spectroscopy," Rev. Sci. Instrum. **82**(6), 063105 (2011).

6. D. B. Foote, M. J. Cich, W. C. Hurlbut, *et al.*, "High-resolution, broadly-tunable mid-IR spectroscopy using a continuous wave optical parametric oscillator," Opt. Express **29**(4), 5295–5303 (2021).

7. A. K. Y. Ngai, S. T. Persijn, G. von Basum, *et al.*, "Automatically tunable continuous-wave optical parametric oscillator for high-resolution spectroscopy and sensitive trace-gas detection," Appl. Phys. B **85**(2-3), 173–180 (2006).

8. J. Peltola, M. Vainio, T. Hieta, *et al.*, "High sensitivity trace gas detection by cantilever-enhanced photoacoustic spectroscopy using a mid-infrared continuous-wave optical parametric oscillator," Opt. Express **21**(8), 10240–10250 (2013).

9. L.-A. Wu, H. J. Kimble, J. L. Hall, *et al.*, "Generation of squeezed states by parametric down conversion," Phys. Rev. Lett. **57**(20), 2520–2523 (1986).

10. L. Davidovich, "Sub-poissonian processes in quantum optics," Rev. Mod. Phys. **68**(1), 127–173 (1996).

11. A. G. White, T. C. Ralph, and H.-A. Bachor, "Active versus passive squeezing by second-harmonic generation," J. Opt. Soc. Am. B **13**(7), 1337–1346 (1996).

12. D. J. M. Stothard, J.-M. Hopkins, D. Burns, *et al.*, "Stable, continuous-wave, intracavity, optical parametric oscillator pumped by a semiconductor disk laser (VECSEL)," Opt. Express **17**(13), 10648–10658 (2009).

13. M. Kuznetsov, F. Hakimi, R. Sprague, *et al.*, "High-power (>0.5-W CW) diode-pumped vertical-external-cavity surface-emitting semiconductor lasers with circular TEM$_{00}$ beams," IEEE Photon. Technol. Lett. **9**(8), 1063–1065 (1997).

14. S. Calvez, J. E. Hastie, M. Guina, *et al.*, "Semiconductor disk lasers for the generation of visible and ultraviolet radiation," Laser Photonics Rev. **3**(5), 407–434 (2009).

15. M. Guina, A. Rantamäki, and A. Härkönen, "Optically pumped VECSELs: review of technology and progress," J. Phys. D: Appl. Phys. **50**(38), 383001 (2017).

16. N. Hempler, G. Robertson, C. Hamilton, *et al.*, "Advances in narrow-linewidth, continuous wave, semiconductor disk laser pumped optical parametric oscillators," in *Proc. SPIE - VECSELs II*, 8242 (2012).

17. P. H. Moriya, Y. Singh, K. Bongs, *et al.*, "Sub-kHz-linewidth VECSELs for cold atom experiments," Opt. Express **28**(11), 15943–15953 (2020).

18. M. Y. A. Raja, S. R. J. Brueck, M. Osiński, *et al.*, "Resonant periodic gain surface-emitting semiconductor lasers," IEEE J. Quantum Electron. **25**(6), 1500–1512 (1989).

19. R. L. Rincon Celis and M. Martinelli, "Reducing the phase noise in diode lasers," Opt. Lett. **44**(13), 3394–3397 (2019).

20. M. Ebrahim-Zadeh, "Continuous-wave optical parametric oscillators," in *Handbook of Optics*, vol. IV, M. Bass, ed. (McGraw-Hill, 2010), pp. 1–33.

21. M. Yamada, N. Nada, M. Saitoh, *et al.*, "First-order quasi-phase matched LiNbO$_3$ waveguide periodically poled by applying an external field for efficient blue second-harmonic generation," Appl. Phys. Lett. **62**(5), 435–436 (1993).

22. X. P. Hu, P. Xu, and S. N. Zhu, "Engineered quasi-phase-matching for laser techniques [Invited]," Photonics Res. **1**(4), 171–185 (2013).

23. S. Guha, F.-J. Wu, and J. Falk, "The effects of focusing on parametric oscillation," IEEE J. Quantum Electron. **18**(5), 907–912 (1982).

24. S. Guha, "Focusing dependence of the efficiency of a singly resonant optical parametric oscillator," Appl. Phys. B **66**(6), 663–675 (1998).

25. N. P. Barnes and V. J. Corcoran, "Parametric generation processes: spectral bandwidth and acceptance angles," Appl. Opt. **15**(3), 696–699 (1976).

26. O. Gayer, Z. Sacks, E. Galun, *et al.*, "Temperature and wavelength dependent refractive index equations for MgO-doped congruent and stoichiometric LiNbO$_3$," Appl. Phys. B **91**(2), 343–348 (2008).

27. D. J. M. Stothard, "Practical continuous-wave intracavity optical parametric oscillators," in *Advances in Optical and Photonic Devices*, K. Y. Kim, ed. (INTECH, 2010), pp. 293–328.

28. F. G. Colville, M. H. Dunn, and M. Ebrahim-Zadeh, "Continuous-wave, singly resonant, intracavity parametric oscillator," Opt. Lett. **22**(2), 75–77 (1997).

29. M. Ebrahim-Zadeh and M. H. Dunn, "Optical parametric oscillators," in *Handbook of Optics*, vol. IV, M. Bass, ed. (McGraw-Hill, 2000), pp. 2201–2272.

30. M. Ebrahimzadeh, G. A. Turnbull, T. J. Edwards, *et al.*, "Intracavity continuous-wave singly resonant optical parametric oscillators," J. Opt. Soc. Am. B **16**(9), 1499–1511 (1999).

31. Y. Yu, X. Chen, L. Cheng, *et al.*, "Continuous-wave intracavity multiple optical parametric oscillator using an aperiodically poled lithium niobate around 1.57 and 3.84 μm," IEEE Photonics J. **9**(2), 1–8 (2017).

32. T. J. Edwards, G. A. Turnbull, M. H. Dunn, *et al.*, "Continuous-wave, singly-resonant, optical parametric oscillator based on periodically poled KTiOPO$_4$," Opt. Express **6**(3), 58–63 (2000).

33. Y. Li, Z. Ding, P. Liu, *et al.*, "Widely tunable, continuous-wave, intra-cavity optical parametric oscillator based on an Yb-doped fiber laser," Opt. Lett. **43**(21), 5391–5394 (2018).

34. K. Devi, S. C. Kumar, and M. Ebrahim-Zadeh, "High-power, continuous-wave, single-frequency, all-periodically-poled, near-infrared source," Opt. Lett. **37**(24), 5049–5051 (2012).

35. M. K. Shukla and R. Das, "High-power single-frequency source in the mid-infrared using a singly resonant optical parametric oscillator pumped by Yb-fiber Laser," IEEE J. Sel. Top. Quantum Electron. **24**(5), 1–6 (2018).

36. G. K. Samanta, G. R. Fayaz, and M. Ebrahim-Zadeh, "1.59W, single-frequency, continuous-wave optical parametric oscillator based on MgO:sPPLT," Opt. Lett. **32**(17), 2623–2625 (2007).

37. A. J. Kemp, G. J. Valentine, J.-M. Hopkins, *et al.*, "Thermal management in vertical-external-cavity surface-emitting lasers: finite-element analysis of a heatspreader approach," IEEE J. Quantum Electron. **41**(2), 148–155 (2005).

38. X.-H. Zheng, G.-Y. He, Z.-X. Jiao, *et al.*, "Stable, high-average-power, continuous-wave singly resonant optical parametric oscillation based on angle-polished MgO:PPLN," J. Infrared Millim. Waves **34**(6), 684–687 (2015).

39. C. Fabre, E. Giacobino, A. Heidmann, *et al.*, "Noise characteristics of a non-degenerate optical parametric oscillator - application to quantum noise reduction," J. Phys. **50**(10), 1209–1225 (1989).

40. D. Cuozzo and G.-L. Oppo, "Two-color continuous-variable quantum entanglement in a singly resonant optical parametric oscillator," Phys. Rev. A **84**(4), 043810 (2011).

41. A. S. Villar, M. Martinelli, and P. Nussenzveig, "Testing the entanglement of intense beams produced by a non-degenerate optical parametric oscillator," Opt. Commun. **242**(4-6), 551–563 (2004).

42. P. H. Moriya, R. Casula, G. A. Chappell, *et al.*, "InGaN-diode-pumped AlGaInP VECSEL with sub-kHz linewidth at 689 nm," Opt. Express **29**(3), 3258–3268 (2021).

43. P. H. Moriya, M. Lee, and J. E. Hastie, "Low phase noise operation of a cavity-stabilized 698 nm AlGaInP-based VECSEL," Opt. Express **31**(17), 28018–28025 (2023).

44. Y.-H. Lai, A. E. Amili, D. Eliyahu, *et al.*, "Ultra-narrow-linewidth Lasers for quantum applications," in *CLEO: Science and Innovations, Technical Digest* (Optica Publishing Group, 2022), STu5O.2.

45. K. Niizeki, K. Ikeda, M. Zheng, *et al.*, "Ultrabright narrow-band telecom two-photon source for long-distance quantum communication," Appl. Phys. Express **11**(4), 042801 (2018).

46. G. Bertaina, C. Clivati, S. Donadello, *et al.*, "Phase noise in real-world twin-field quantum key distribution," ArXiv, ArXiv:2310.08621v1 (2023).

47. C. Lindner, J. Kunz, S. J. Herr, *et al.*, "High-sensitivity quantum sensing with pump-enhanced spontaneous parametric down-conversion," APL Photonics **8**(5), 051301 (2023).

48. D. Nie, J. Feng, Y. Li, *et al.*, "Two-color quantum correlation between down-conversion beams at 1.5 and 3.3 μm from a singly resonant optical parametric oscillator," Appl. Sci. **10**(8), 2698 (2020).

49. N. Akerman, N. Navon, S. Kotler, *et al.*, "Universal gate-set for trapped-ion qubits using a narrow linewidth diode laser," New J. Phys. **17**(11), 113060 (2015).

50. S. Anderson, P. H. Moriya, L. Caspani, *et al.*, "Data for: "Single-frequency optical parametric oscillator intracavity-pumped by a visible VECSEL for low-noise down-conversion to 1.55 μm"," Unviersity of Strathclyde (2023). DOI: https://doi.org/10.15129/9fff8e03-d6c0-4164-a258-01a5d4469f39 .